目錄

中文摘要

由於氫鍵的立體網絡，水的結構、動態、及性質是非常複雜。在密閉空間的水和生物學更有關連性，這是因為生物性質的水通常限制在細胞器或是奈米至微米比例的細胞中。儘管過去在瞭解水的性質上已從事很多努力，水仍然給我們留下未解的實質。我們對密閉性質的水仍然所知不多。水的複雜度呈現於不同的物理及化學現象中，其中一項就是觀測於水中的振動光譜間不均勻擴增的 O-H 伸縮振動範圍。O-H 伸縮振動範圍在被水分子環繞的環境中有所反應，故 O-H 伸縮振動範圍能作為好的探測工具讓我們在分子的層級中瞭解水。

目前此研究計畫的主要目標是研究外部應用電場在水的 O-H 伸縮振動範圍上的反應。關於這項研究，紅外線電場變調吸收光譜是最能顯現其能力的技術。我們實驗室在紅外線吸收光譜的獨特設備上，能測量外加電場感應的紅外線吸光度之變動小至 10^{-7}。紅外線電場變調提供固定且難得的資訊在分子性質上，例如：永久偶極矩及可極化率。因為水是有機分子，它會藉著靜電反應在電場中反應。甚者，在明顯的氫鍵環境中，在水種類的平衡改變也會發生。

我們已經在兩種環境中進行紅外光電場對水的測量：一種是水溶解在 1,4-二氧陸圜，另一種則是水在磺酸基琥珀酸鈉(AOT)的逆微膠粒中。在水濃度低於 2.0M 的 1,4-二氧陸圜溶液中，水分子主要環繞於 1,4-二氧陸圜溶液中，此在 AOT 逆微膠粒中，其處於由界面活性劑組成的奈米微水池中。我們已成功取得這兩樣樣本，由水中的紅外線電場光譜的氫鍵中得到合理的訊雜比。就我們所認知的，這是首次在水的液態中觀測到紅外線電場。這項結果顯示紅外線電場變調在 1,4-二氧陸圜氫鍵的訊號對過渡性極化度有顯著的貢獻，且和我們目前至今所研究的液體成果可做對照。紅外線電場光譜在 AOT 逆微膠粒的水中和 1,4-二氧陸圜溶液的水中是非常不一樣的。我們已經發現紅外線電場變調的信號起源於存在微水池中三種明顯水種類的平衡改變。我們實驗的結果似乎顯示出禁錮水的質性可能被外加電場所控制。我們相信目前尋得的結果將會提供確據的研究平台在探查水的狀況上，而這同時也是我們實驗室目前計畫處理的。

我們同時提出另一項計畫，這計畫是利用電場調變紅外線吸收光譜研究 N,N-Dimethyl-p-nitroaniline 在混合溶液乙晴中的實驗。和硝苯胺不同，DMPNA 和乙晴在溶液中時，並不會形成特定的溶解結構。更有趣的是，我們發現大部分在水溶液裡的乙晴分子產生成雙體結體，且其二聚體為頭對尾相接線性結構。我們感到驚訝原因在於另一種雙體結構，反平行結構，已經知道至少在氣體狀態下是比較穩定的。

中文關鍵詞

水，電場調變紅外線吸收光譜，逆微胞，偶極矩

英文摘要

The structure and dynamics of bulk water are exceedingly complex due to the three-dimensional network of hydrogen bonds. Water in confinement is more relevant to biology. Despite a great deal of efforts, water still remains a mysterious substance to us. We know far less about water in confinement. The complexity of water is manifested in various physical and chemical phenomena, one of which is the inhomogeneously broadened O–H stretch band observed in the vibrational spectrum of water. The O–H stretch band sharply reflects the local environment around a water molecule, so it is a good probe to understand water at the molecular level.

The primary objective of this project is to study the effects of an externally applied electric field on the O–H stretch band of water. IR electroabsorption spectroscopy is one of the most powerful techniques for such studies. Our unique apparatus can measure changes in IR absorbance induced by the applied electric field as small as 10^{-7}. This technique provides quantitative and otherwise unobtainable information on molecular properties such as the permanent dipole moment and polarizability.

We have carried out IR electroabsorption measurements of water in two different environments: water dissolved in 1,4-dioxane and water in AOT reverse micelles. In 1,4-dioxane solution (<2.0 M), a water molecule is surrounded mainly by 1,4-dioxane molecules, whereas in the AOT reverse micelle, it resides within a nanoscopic water pool formed by the surfactant. We have succeeded in recording for both samples the IR electroabsorption spectrum in the O–H stretch region with reasonable S/N. To our knowledge, this is the first observation of IR electroabsorption of water in the solution phase. The IR electroabsorption signal of the O–H stretch band of water in 1,4-dioxane has a significant contribution of the transition polarizability, in contrast to other liquids we have so far studied. The IR electroabsorption spectrum of water in the AOT reverse micelle is quite different from that of water in the 1,4-dioxane solution. We have found that the IR electroabsorption signal

originates from the equilibrium change between three distinct water species present in the water pool.

We also report on another project of IR electroabsorption spectroscopy of *N*,*N*-dimethyl-*p*-nitroaniline (DMPNA) in acetonitrile/C_2Cl_4.

英文關鍵詞

Water, infrared electroabsorption spectroscopy, reverse micelle, dipole moment

報告內容

1. Project I: Infrared electroabsorption study of water

1.1. Introduction

Water, the most abundant liquid in nature, plays essential roles in virtually all scientific disciplines. Despite much effort, a detailed microscopic picture of water remains to be obtained. In the vibrational spectrum of water, the O–H stretch ν(OH) transition of water appears as an intense, inhomogeneously broadened band. Because of the featureless band profile, few clues can be derived from the steady-state ν(OH) absorption spectrum alone. More insights can be gained *e.g.* by studying water's responses to an external perturbation. Here, we employ the application of an external electric field and study its effects on absorption spectra [1,2] (*i.e.*, electroabsorption spectroscopy), particularly in the IR region. Because water is polar (μ_P = 2–3 D [3]), it is expected to respond to an externally applied electric field *via* electrostatic interactions.

There are several technical difficulties in IR electroabsorption measurements on water. Water has a considerably large dielectric constant ($\varepsilon \approx 80$), possibly causing a large voltage drop and phase retardation at an electric contact. In addition, the molar extinction coefficient of the ν(OH) band of water is so large that the transmittance in the ν(OH) region can easily fall below the detection limit of the apparatus. A simple remedy for this problem would be to make the sample extremely thin, typically thinner than 1 μm [4]. However, it would be inconvenient to employ such a thin sample cell. Instead, we here alleviate the problem by effectively decreasing the concentration of water in two different ways. One approach is to dilute water with a solvent. In this work, 1,4-dioxane, an aprotic solvent with nearly zero dipole moment, is used as the solvent (Fig. 1-1a).

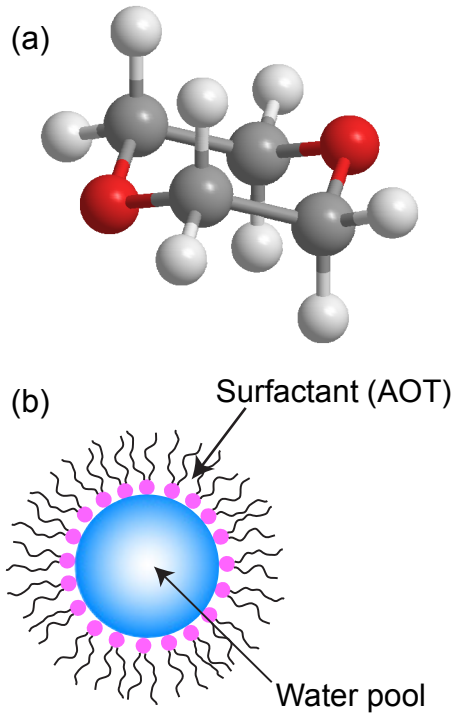

Figure 1-1: (a) 1,4-Dioxane. (b) Schematic illustration of an AOT reverse micelle. Water is confined to a nanoscale pocket formed by the surfactant molecules.

The other approach is to confine water to the nanopool of the reverse micelle of 1,4-bis(2-ethylhexoxy)-1,4-dioxobutane-2-sulfonate (AOT; see Fig. 1-1b) [5–10]. We can control the size of the water pool by varying the molar ratio

$$w_0 = [\mathrm{H_2O}]/[\mathrm{AOT}]. \tag{1-1}$$

Not only does this approach effectively decrease water concentration, but it will also allow us to compare the effect of confining water to the reverse micelle with that of dissolving water in a solvent. The two approaches will serve as a bottom-up approach to understand the anomaly of water because the complexity associated with the hydrogen-bonding network present in bulk water may be reduced.

1.2. Theoretical background

A general theory of electroabsorption was established by Liptay and co-workers [1]. The $\Delta A(\tilde{\nu})$ spectrum can be formulated as [2,11]

$$\Delta A(\tilde{\nu}) = F^2 \left[A_\chi A(\tilde{\nu}) + \frac{B_\chi}{15hc} \tilde{\nu} \frac{\mathrm{d}}{\mathrm{d}\tilde{\nu}} \frac{A(\tilde{\nu})}{\tilde{\nu}} + \frac{C_\chi}{30h^2c^2} \tilde{\nu} \frac{\mathrm{d}^2}{\mathrm{d}\tilde{\nu}^2} \frac{A(\tilde{\nu})}{\tilde{\nu}} \right] \tag{1-2}$$

where F is the internal electric field, h is Planck's constant, and c is the speed of light. There are also third derivative and higher order terms in Eq. 1-2, but they are all proportional to the fourth or higher powers of the electric field, which we do not detect. $\Delta A(\tilde{\nu})$ comprises the zeroth, first, and second derivatives of the absorption band $A(\tilde{\nu})$. For a randomly oriented, mobile molecule, the coefficients A_χ, B_χ, and C_χ are given by [11]

$$\begin{aligned} A_\chi = {} & \frac{1}{30|\mathbf{m}|^2} \sum_{ij} \left[10A_{ij}{}^2 + \left(3A_{ii}A_{jj} + 3A_{ij}A_{ji} - 2A_{ij}{}^2 \right) \left(3\cos^2\chi - 1 \right) \right] \\ & + \frac{1}{15|\mathbf{m}|^2 k_\mathrm{B}T} \sum_{ij} \left[10m_i A_{ij} \mu_{\mathrm{g}j} + \left(3m_i A_{ji} \mu_{\mathrm{g}j} + 3m_i A_{jj} \mu_{\mathrm{g}i} - 2m_i A_{ij} \mu_{\mathrm{g}j} \right) \left(3\cos^2\chi - 1 \right) \right] \\ & + \frac{1}{10k_\mathrm{B}T} \left(\alpha_{\mathrm{gm}} - \overline{\alpha_\mathrm{g}} \right) \left(3\cos^2\chi - 1 \right) + \frac{\mu_\mathrm{g}{}^2}{30k_\mathrm{B}^2T^2} \left(3\cos^2\alpha - 1 \right) \left(3\cos^2\chi - 1 \right) \end{aligned} \tag{1-3}$$

$$\begin{aligned} B_\chi = {} & \frac{1}{|\mathbf{m}|^2} \sum_{ij} \left[m_i A_{ij} \Delta\mu_j + \left(3m_i A_{ji} \Delta\mu_j + 3m_i A_{jj} \Delta\mu_i - 2m_i A_{ij} \Delta\mu_j \right) \left(3\cos^2\chi - 1 \right) \right] \\ & + \frac{15}{2} \overline{\Delta\alpha} + \frac{3}{2} \left(\Delta\alpha_\mathrm{m} - \overline{\Delta\alpha} \right) \left(3\cos^2\chi - 1 \right) + \frac{5}{k_\mathrm{B}T} \left(\boldsymbol{\mu}_\mathrm{g} \cdot \Delta\boldsymbol{\mu} \right) \\ & + \frac{1}{k_\mathrm{B}T} \left[3 \left(\hat{\mathbf{m}} \cdot \boldsymbol{\mu}_\mathrm{g} \right) \left(\hat{\mathbf{m}} \cdot \Delta\boldsymbol{\mu} \right) - \left(\boldsymbol{\mu}_\mathrm{g} \cdot \Delta\boldsymbol{\mu} \right) \right] \left(3\cos^2\chi - 1 \right) \end{aligned} \tag{1-4}$$

$$C_\chi = 5\left|\Delta\boldsymbol{\mu}\right|^2 + \left[3\left(\hat{\mathbf{m}}\cdot\Delta\boldsymbol{\mu}\right) - \left|\Delta\boldsymbol{\mu}\right|^2\right]\left(3\cos^2\chi - 1\right) \tag{1-5}$$

where the transition hyperpolarizability **B** is neglected. $\boldsymbol{\mu}_g$ is equivalent to $\boldsymbol{\mu}_p$. **A** denotes the transition polarizability. $\Delta\boldsymbol{\mu}$ and $\Delta\boldsymbol{\alpha}$ denote the changes in dipole moment and polarizability tensor between the vibrational ground state (g) and an excited state (e), respectively, *i.e.*, $\Delta\boldsymbol{\mu} = \boldsymbol{\mu}_e - \boldsymbol{\mu}_g$ and $\Delta\boldsymbol{\alpha} = \boldsymbol{\alpha}_e - \boldsymbol{\alpha}_g$. $\hat{\mathbf{m}}$ is a unit vector in the direction of the transition moment **m**. α_{gm} and $\Delta\alpha_m$ are the components of the ground-state polarizability and the polarizability change along the direction of the transition moment, *i.e.*, $\alpha_{gm} = \hat{\mathbf{m}}\cdot\boldsymbol{\alpha}_g\cdot\hat{\mathbf{m}}$ and $\Delta\alpha_m = \hat{\mathbf{m}}\cdot\Delta\boldsymbol{\alpha}\cdot\hat{\mathbf{m}}$. A bar indicates the average value of the polarizability ($\overline{\alpha_g} = \frac{1}{3}\mathrm{Tr}\alpha_g$, $\overline{\Delta\alpha} = \frac{1}{3}\mathrm{Tr}\Delta\alpha$).

The zeroth-derivative term represents the *intensity change* of the absorption spectrum. The first-derivative term depends on both $\Delta\boldsymbol{\mu}$ and $\Delta\boldsymbol{\alpha}$ and is responsible for the *peak shift*. The second-derivative term, which is characterized solely by $\Delta\boldsymbol{\mu}$, shows the *change in the band width* of the absorption spectrum.

1.3. Method—IR electroabsorption spectroscopy

Figure 1-2 shows a schematic illustration of the IR electroabsorption spectrometer used in this study [12–14]. A ceramic IR emitter was used as the mid-IR light source. The absorption spectrum of the sample was measured with a dispersive IR monochromator and an InSb detector, and recorded on a digital sampling oscilloscope. In measuring the ΔA spectrum of the sample, the alternating current (AC) coupled amplification was employed that was developed previously for time-resolved IR spectroscopy, followed by phase sensitive detection with a lock-in amplifier. The combined use of the dispersive monochromator and the AC-coupled amplifier in our apparatus enables detection of ΔA as small as 10^{-7} [12]. A 25 kHz sinusoidal AC voltage generated by a function generator was applied across the sample cell, in which p-type boron-doped silicon plates (thickness = 0.5 mm, resistivity = 0.8–2 Ω cm) were used as both optical windows and electrodes. The silicon plates transmitted >50% of light in the

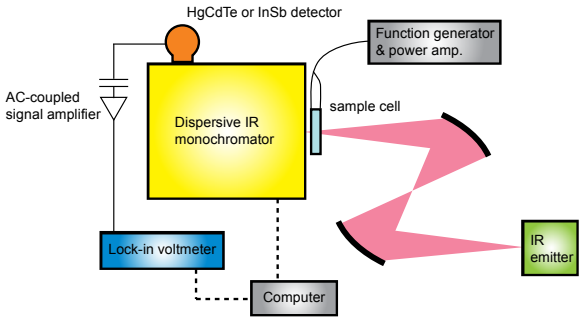

Figure 1-2: Schematic illustration of the IR electroabsorption spectrometer. In this work, an InSb detector was used.

1000–2000 cm^{-1} region. To avoid applying a high voltage, the cell gap was kept typically below 10 μm by using a 6-μm-thick polyethylene terephthalate film as a spacer. The lock-in amplifier detected only the AC signal component modulated at 50 kHz, twice the frequency of the applied electric field, yielding the second-order Stark spectrum. Angle χ dependence of ΔA spectra was studied using p-polarized IR light obtained with a wire-grid polarizer. IR spectra were also recorded on a JASCO FT/IR-6100 spectrometer, *the major equipment that we purchased using the present research grant*, using a sample cell composed of two CaF_2 windows and a 50 μm lead spacer. All measurements were performed at room temperature.

1.4. Results and discussion

1.4.1. Water in 1,4-dioxane [15]

A. Concentration dependence of FT-IR spectra

Figure 1-3a shows FT-IR spectra in the 3000–3800 cm^{-1} region of water dissolved in 1,4-dioxane at molar concentrations of 0.25, 0.50, 0.75, 1.0, 1.25, 1.5, 1.75, and 2.0 M. A major broad feature, which apparently consists of two peaks, is observed at ~3550 cm^{-1}. This band is unambiguously assigned to the O–H stretch of water. There is a small hump at around 3260 cm^{-1} (see, for example, the 2.0 M spectrum). This band is assigned to the first overtone of the O–H bend, 2δ(OH). The band shape of the ν_{OH} band is found to change with water concentration. To better see the change, we normalized the absorption spectra to the peak height at 3514 cm^{-1}. Figure 1-3b shows the resulting normalized spectra. As the concentration increases, the higher-wavenumber peak of the ν_{OH} band decreases in intensity and, concomitantly, the lower-wavenumber side of the band appears to be broadened.

We also measured the concentration dependence of FT-IR spectra of water in 1,4-dioxane at lower concentrations (0.05, 0.10, 0.15, 0.20, 0.25, 0.30, 0.35, and 0.40 M). Figure 1-4a,b shows the spectra with and without normalization to the peak height at 3514 cm^{-1}, respectively. As can be seen from Fig. 1-4a, the band shape of the ν(OH) band and the intensity ratio of its two peaks look quite similar in this concentration range. However, the normalized spectra (Fig. 1-4b) do exhibit the same tendency as in Fig. 1-3b, although somewhat less prominent. These results indicate that the water species responsible for the observed ν_{OH} band may exist even at low concentrations (<0.40 M).

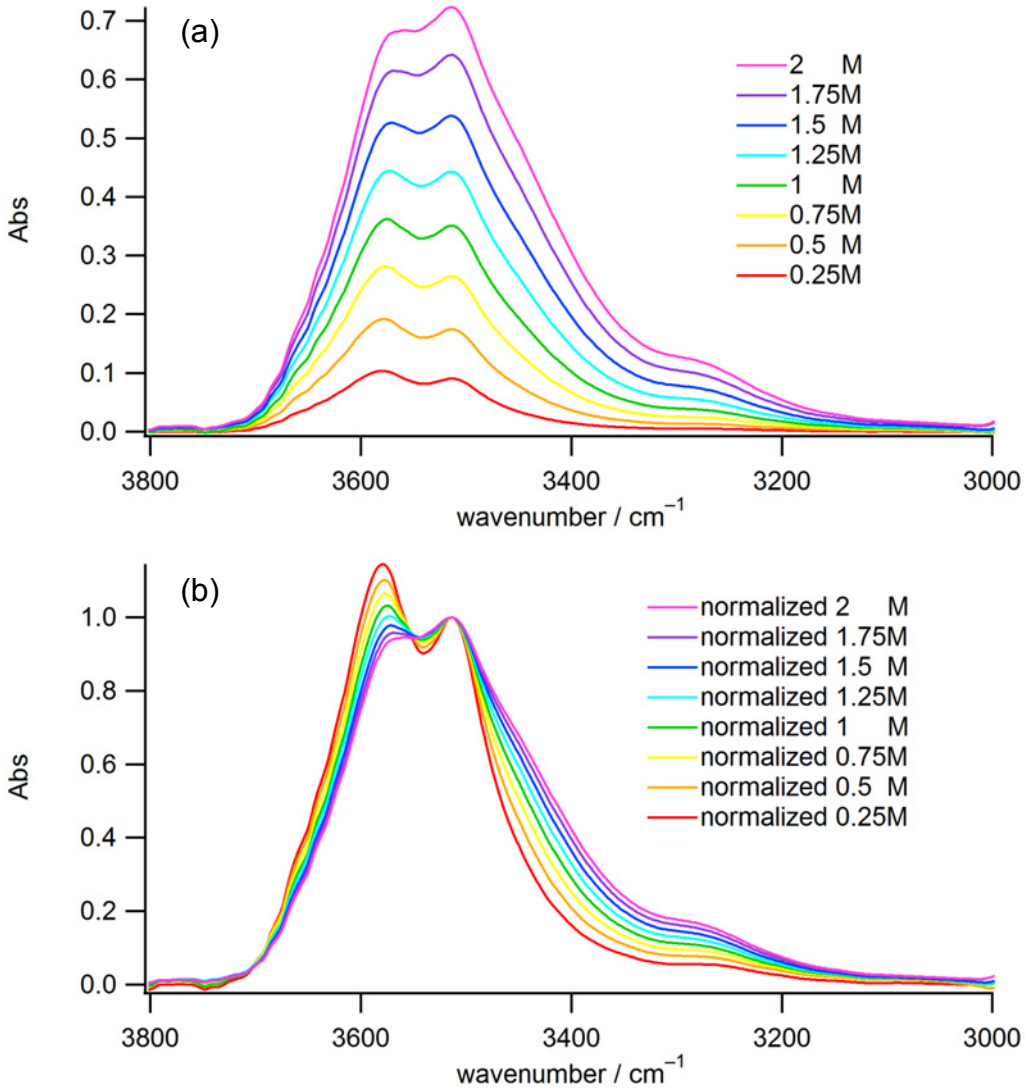

Figure 1-3: (a) Concentration dependence of FT-IR spectra in the 3000–3800 cm^{-1} region, of water dissolved in 1,4-dioxane at eight different concentrations. (b) The same spectra as in part (a) but normalized to the peak height at 3514 cm^{-1}.

To extract the intrinsic IR spectra of the water species in the 1,4-dioxane solution in the concentration range studied, we analyzed the spectra data using non-negative matrix factorization (NMF) [16]. In NMF analysis, a data matrix **X** of a series of spectra at different concentrations is decomposed into physically meaningful matrices **H** and **W**. The matrix **H** contains normalized concentration profiles of individual molecular components and the matrix **W** contains the corresponding intrinsic spectra. The sum squared residual $|| \mathbf{X} - \mathbf{H}\mathbf{W}^{T} ||$ is minimized by solving alternating least-squares problems iteratively under the constraint that concentration and spectral intensity (*i.e.*, the matrix elements of **H** and **W**) are non-negative. Before running NMF, we need to presume the number of components. Here, we

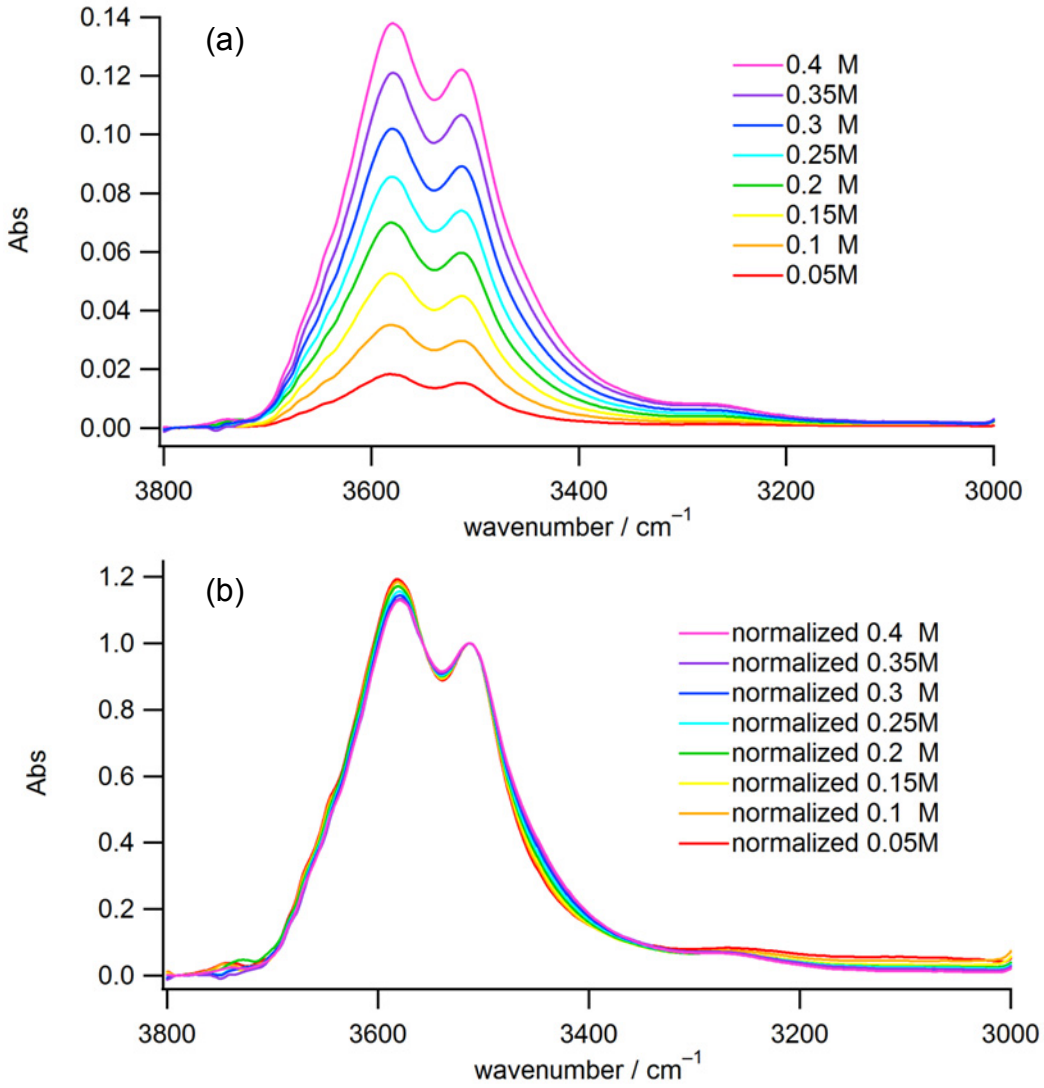

Figure 1-4: (a) Concentration dependence of FT-IR spectra in the 3000–3800 cm^{-1} region, of water dissolved in 1,4-dioxane at eight different concentrations below 0.4 M. (b) The same spectra as in part (a) but normalized to the peak height at 3514 cm^{-1}.

refer to the result of singular value decomposition (SVD) of the dataset shown in Fig. 1-3a. The SVD result shows that there are two principal singular values. We thus set the number of components required in NMF as two. Hereafter the major component will be denoted 1 and the minor 2. A randomly generated basis was used as an initial guess for **W**. One thousand iterations were enough to obtain a good convergence regardless of the initial guess.

What molecular models can account for the water components 1 and 2? Because the major component 1 exists even at low concentrations, it would be natural to attribute it to an isolated water molecule surrounded by 1,4-dioxane molecules as illustrated in Fig. 1-5a. On the other hand, we hypothesize that the minor component 2 is assigned to water species inside

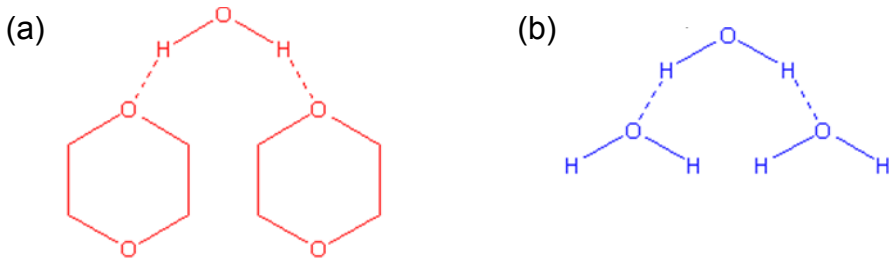

Figure 1-5: Models for the water components 1 and 2. (a) The major component 1 is an isolated water molecule surrounded by 1,4-dioxane molecules. (b) The minor component 2 is a water molecule inside a small cluster of water. This water molecule forms hydrogen bonds with neighboring water molecules in the ensemble and/or 1,4-dioxane.

a small cluster of water molecules that forms hydrogen bonds with neighboring water molecules or 1,4-dioxane molecules outside the cluster (see Fig. 1-5b).

The concentration profiles ($\mathbf{h}_1$ and $\mathbf{h}_2$) and intrinsic spectra ($\mathbf{w}_1$ and $\mathbf{w}_2$) of components 1 and 2 derived from the NMF analysis are displayed in Fig. 1-6. As expected, the w_1 spectrum explains the major feature of the O–H stretch band of water, in which two peaks at around 3600 and 3500 cm^{-1} are dominant. The two peaks are reminiscent of the antisymmetric and symmetric O–H stretches, ν_{as}(OH) and ν_s(OH), of water. It is not surprising that the w_1 spectrum shows two distinct ν(OH) peaks in contrast with the broad, featureless ν(OH) band of pure liquid water, because component 1 has been considered in our model as an isolated water molecule in the 1,4-dioxane medium. In this sense, the w_1 spectrum is consistent with our model of water. We fit the w_1 spectrum to a sum of three Lorentzian functions plus a baseline represented by a linear function. The two Lorentzian functions at higher wavenumbers

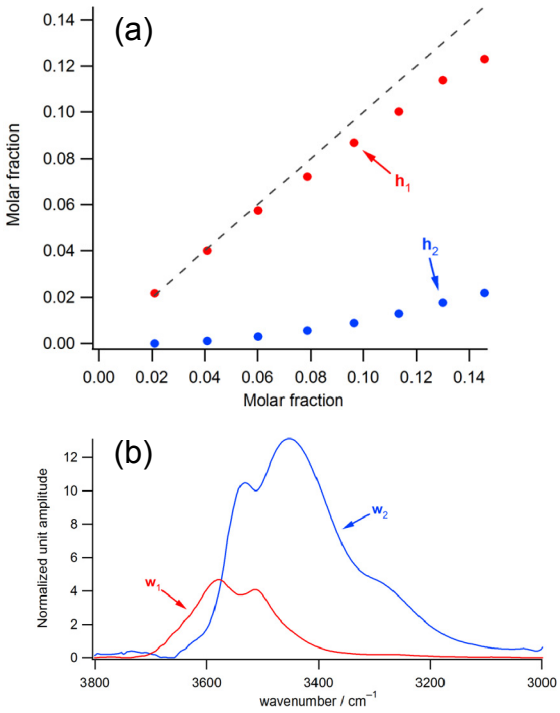

Figure 1-6: The results of NMF analysis under the assumption that there are two water components present in 1,4-dioxane solution. (a) Mole fraction profiles (h_1 and h_2). The dashed line represents the sum of $\mathbf{h_1}$ and $\mathbf{h_2}$. (b) Intrinsic spectra (w_1 and w_2).

account for the ν_{as}(OH) and ν_s(OH) bands, and the third one with very small intensity for the first overtone of δ(OH). The best fit is shown in Fig. 1-7a, and the peak positions and band widths (FWHM) of the three bands are given in Table 1-1.

Table 1-1: Peak positions and band widths determined by the fitting of the w_1 spectrum (Fig. 1-7a).

	Peak position (cm^{-1})	Band width (cm^{-1})
Lorentzian 1	3589	84
Lorentzian 2	3507	99
Lorentzian 3	3262	80

The w_2 spectrum shows a more complicated band profile, which has a maximum at a lower wavenumber relative to the w_1 spectrum and includes at least three peaks. The profile of the w_2 spectrum resembles the inhomogeneously broadened ν(OH) band of pure water. This similarity in spectral profile is consistent with our model for component 2, in which the component is assigned to a water molecule in a water cluster. In fact, the w_2 spectrum can be well reproduced by a sum of two Gaussian functions and one Lorentzian function (plus a baseline) rather than a sum of three Lorentzian functions, implying inhomogeneous characteristics of the w_2 spectrum. The best fit is shown in Fig. 1-7b, and the peak positions and band widths (FWHM) of the three bands are given in Table 1-2.

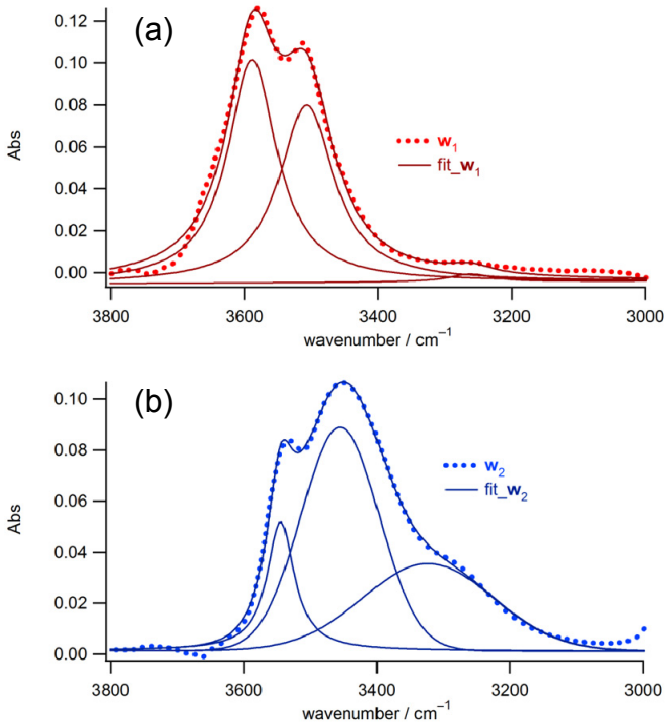

Figure 1-7: (a) Concentration dependence of FT-IR spectra in the 3000–3800 cm^{-1} region, of water dissolved in 1,4-dioxane at eight different concentrations below 0.4 M. (b) The same spectra as in part (a) but normalized to the intensity at 3514 cm^{-1}.

Table 1-2: Peak positions and band widths determined by the fitting of the $\mathbf{w}_2$ spectrum (Fig. 1-7b).

	Peak position (cm^{-1})	Band width (cm^{-1})
Lorentzian 1	3545	49
Gaussian 1	3456	138
Gaussian 2	3323	231

B. Angle χ dependence of IR electroabsorption spectra

Figure 1-8 shows the ΔA spectra in the ν(OH) region of water in 1,4-dioxane (1.0 M, F_{ext} = 1.17×10^7 V m^{-1}) at five different angles χ = 55°, 63°, 72°, 81°, and 90°. ΔA signals in the O–H stretch region as small as 1×10^{-6} have been successfully detected for the first time. At χ = 90° (normal incidence of the IR light to the sample cell), the ν(OH) ΔA spectrum is dominated by a positive peak centered at ~3540 cm^{-1} and a broad dip between 3600 and 3700 cm^{-1}. As χ is varied from 90° to 55° (near the magic angle), the positive peak gradually diminishes, whereas the negative peak remains almost unchanged. Inspection of the singular values obtained from SVD and their intrinsic spectra suggests that the observed χ-dependence of the ΔA spectra in the ν(OH) region can be explained by considering only two components associated with the largest two singular values and disregarding the other components as noises. As in previous studies [12,13], we assume the surviving two components to be constant with respect to χ (χ-independent component) and to behave according to $1-3\cos^2\chi$ (χ-dependent component). By taking a proper linear combination of the vectors based on the model for the χ dependence, we can reconstruct physically meaningful vectors. The reconstructed χ dependences and spectra are shown in Fig. 1-9a,b, respectively. Reconstructed ΔA spectra are overall in good agreement with the observed spectra.

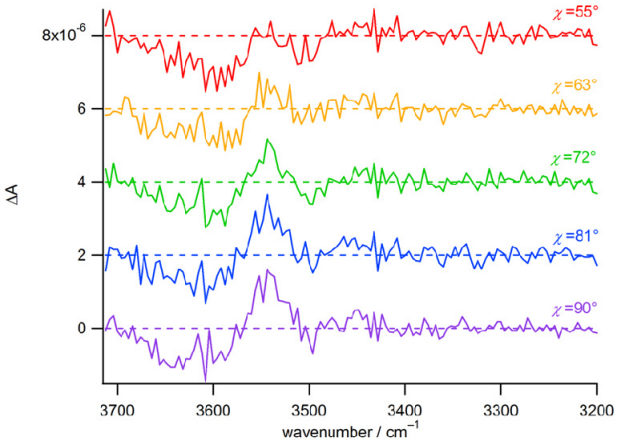

Figure 1-8: IR electroabsorption spectra of water in 1,4-dioxane (1.0 M) measured at χ = 55, 63, 72, 81 and 90°. Each ΔA spectrum is offset by 2×10^{-6} for clarity of display.

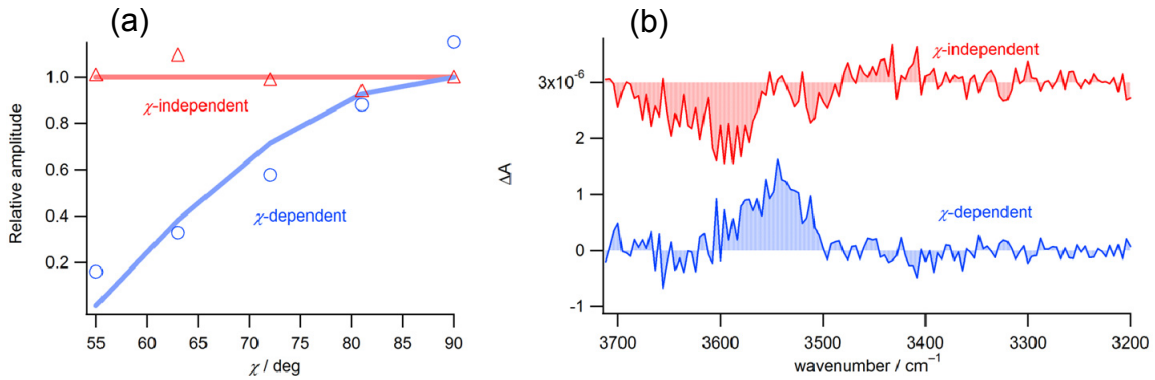

Figure 1-9: (a) Model functions (thick solid line) and reconstructed χ dependences (open triangle and circle). (b) χ-independent (red) and χ-dependent (blue) spectral components.

The χ-dependent component spectrum (blue spectrum in Fig. 1-9b) is dominated by a positive peak centered at ~3540 cm^{-1} with no appreciable negative dip in other regions. Because the χ-dependent component vanishes at around χ = 55°, the χ-independent component spectrum (red spectrum in Fig. 1-9b) is almost identical to the χ = 55° spectrum. It is composed of two negative bands: the larger feature is located at ~3600 cm^{-1}, and the smaller one appears around 3500 cm^{-1}.

C. Fitted results of the χ-independent and χ-dependent component spectra

Next, we fit the χ-independent and χ-dependent component spectra to Eq. 1-2 using the w_1 spectrum composed of two distinct water species determined by the NMF analysis. The concentration-weighted IR spectra of components 1 and 2 (total water

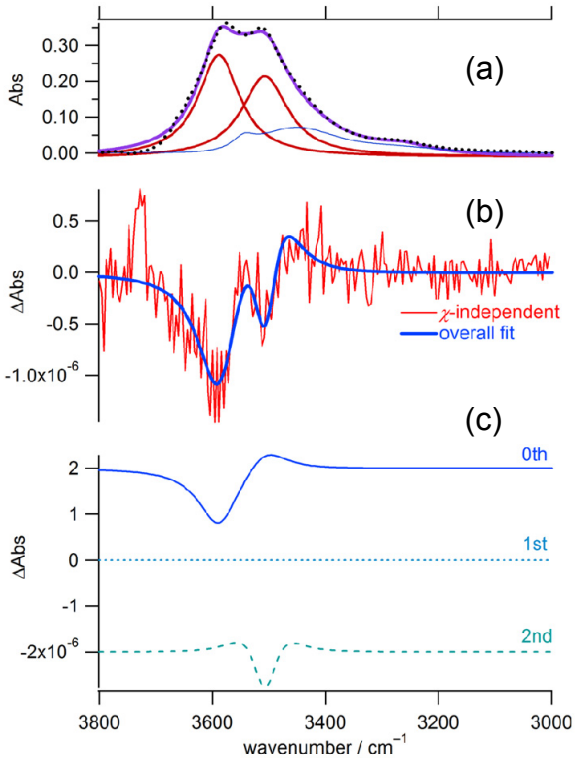

Figure 1-10: Fitted result for the χ-independent component spectrum of water in 1,4-dioxane. (a) Dotted black line, observed FT-IR spectrum; purple solid line, simulated spectrum using the results of NMF analysis (see text for details); red thick solid line, two Lorentzian bands, ν_{as}(OH) and ν_s(OH), consisting of the w_1 spectrum; blue thin solid line, the w_2 spectrum, which is neglected in the fit below. (b) Red line, χ-independent ΔA spectrum obtained with SVD; thick blue line, the best fit to Eq. 1-2. (c) Decomposition of the overall fit into the zeroth (solid line), first (dotted line), and second (dashed line) derivative shapes.

concentration = 1.0 M) are shown in Fig. 1-10a. The peak height of the w_2 spectrum is about four times weaker than that of the two Lorentzian bands consisting of the w_1 spectrum. As a result, the contribution of component 2 to the ΔA spectra is deemed comparable to the noise level ($<0.5 \times 10^{-6}$). We thus make a reasonable approximation that component 2 is neglected in the fitting analysis of the ΔA spectra and only component 1 (*i.e.* antisymmetric and symmetric stretch bands of isolated water) is taken into account. In the fitting, the band widths and peak positions of the ν_{as}(OH) and ν_s(OH) bands are fixed to the values given in Table 1-1. Under these conditions, the χ-independent and χ-dependent component spectra were fit to a linear combination of the zeroth, first, and second derivatives of each absorption band (Lorentzian). The results for the χ-independent and χ-dependent spectra are shown in Fig. 1-10b,c and Fig. 1-11b,c, respectively. The parameters, a_χ, b_χ, and c_χ, for each band determined by the fitting are summarized in Table 1-3. They are related to the coefficients, A_χ, B_χ, and C_χ, in Eq. 1-2 *via* the following equations:

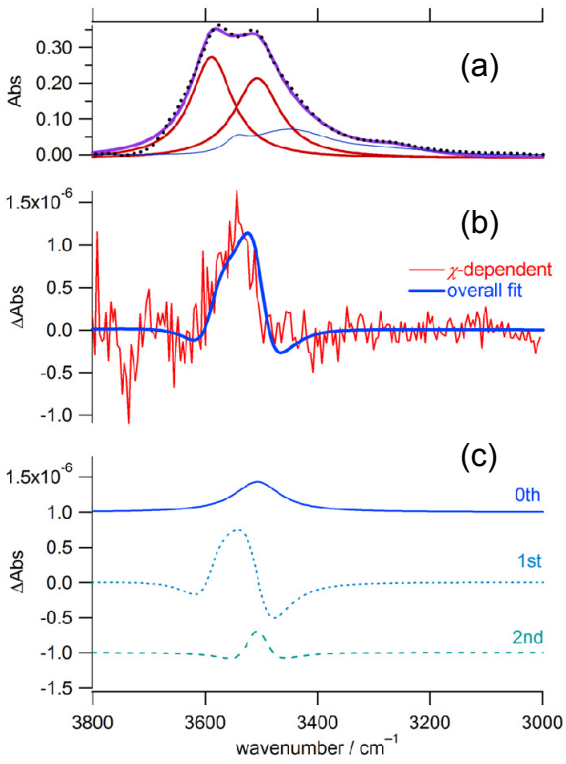

Figure 1-11: Fitted result for the χ-dependent component spectrum of water in 1,4-dioxane. (a) Dotted black line, observed FT-IR spectrum; purple solid line, simulated spectrum using the results of NMF analysis (see text for details); red thick solid line, two Lorentzian bands, ν_{as}(OH) and ν_s(OH), consisting of the w_1 spectrum; blue thin solid line, the w_2 spectrum, which is neglected in the fit below. (b) Red line, χ-dependent ΔA spectrum obtained with SVD; thick blue line, the best fit to Eq. 1-2. (c) Decomposition of the overall fit into the zeroth (solid line), first (dotted line), and second (dashed line) derivative shapes.

$$a_\chi = F^2 A_\chi \tag{1-6}$$

$$b_\chi = \frac{F^2}{15hc} B_\chi = \left(3.356\times10^{23} F^2\right) B_\chi \tag{1-7}$$

$$c_\chi = \frac{F^2}{30h^2c^2} C_\chi = \left(8.447\times10^{47} F^2\right) C_\chi \tag{1-8}$$

Some of the coefficients [*e.g.*, a_χ for the ν_{as}(OH) band in the χ-dependent ΔA spectrum] turned out not to affect the fit, so they were set equal to zero in the spirit of reducing the number of adjustable parameters. In addition, during the fitting, we imposed a relation between the c_χ's for ν_s(OH) of the χ-independent and χ-dependent components (*vide infra*).

Table 1-3. The fitted parameters a_χ, b_χ, and c_χ, of the zeroth, first, and second derivative terms of the χ-dependent and χ-independent ΔA spectra of water in 1,4-dioxane.

	χ-independent ΔA spectrum		χ-dependent ΔA spectrum	
	ν_{as}(OH)	ν_s(OH)	ν_{as}(OH)	ν_s(OH)
a_χ	-4.7×10^{-6}	2.52×10^{-6}	0	1.92×10^{-6}
b_χ	0	0	6.69×10^{-5}	1.87×10^{-4}
c_χ [a]	0	4.22×10^{-3}	0	-1.69×10^{-3}

[a]The parameters for the χ-independent and χ-dependent component spectra are related to each other by Eq. 1-15.

Figures 1-10c and 1-11c reveal the following qualitative features. (i) The χ-independent spectrum is dominated by the zeroth and second derivative components. We conclude that within experimental errors, there is no contribution from the first derivative term. Because the ν_{as}(OH) and ν_s(OH) bands are vibrational modes of the same molecule, an equilibrium shift cannot contribute to the zeroth derivative component in the present case. Therefore, the result seems to suggest a significant contribution of the transition polarizability **A**. (ii) The χ-dependent spectrum has contributions from all the three terms with the first derivative term being dominant. (iii) In the χ-dependent spectrum, the zeroth derivative signal of ν_{as}(OH) is zero and that of ν_s(OH) is positive. This is quite surprising because the ν_{as}(OH) mode (α = 90°) and ν_s(OH) mode (α = 0°) should give positive and negative ΔA signals, respectively, if orientational polarization is the main contributor to the zeroth derivative spectrum, as is often the case [13]. Again, the fitted result is indicative of large contributions of the transition polarizability **A**. (iv) The second derivative signal, which is proportional to $|\Delta\boldsymbol{\mu}|^2$, is zero for the ν_{as}(OH) band but nonzero for the ν_s(OH) band. This can be rationalized in a qualitative manner as follows. The transition moment **m** is perpendicular to $\boldsymbol{\mu}_g$ for ν_{as}(OH), so the $v = 1 \leftarrow 0$ excitation would not alter the dipole moment much, resulting in $\boldsymbol{\mu}_e \approx \boldsymbol{\mu}_g$ and hence $|\Delta\boldsymbol{\mu}| \approx 0$. On the other hand, the transition moment of the ν_s(OH) mode is parallel to $\boldsymbol{\mu}_g$, so the vibrational excitation of this mode would induce a large change in dipole moment, resulting in

$\boldsymbol{\mu}_e \neq \boldsymbol{\mu}_g$ and hence $|\Delta\boldsymbol{\mu}| > 0$.

From the parameters a_χ, b_χ, and c_χ, the values of the molecular properties such as $\Delta\boldsymbol{\mu}$, $\Delta\boldsymbol{\alpha}$, and **A** can, in principle, be obtained using Eqs. 1-3–5, although it is often necessary to make further assumptions or simplifications (*e.g.*, **A** is a symmetric tensor). Each of Eqs. 1-3–5 can be divided into two parts according to the dependence on angle χ. The fragments that show the $3\cos^2\chi - 1$ dependence are

$$\begin{aligned} A_{3\cos^2\chi-1} = {} & \frac{1}{30|\mathbf{m}|^2}\sum_{ij}\left(3A_{ii}A_{jj} + 3A_{ij}A_{ji} - 2A_{ij}^{\,2}\right)\left(3\cos^2\chi - 1\right) \\ & + \frac{1}{15|\mathbf{m}|^2 k_\mathrm{B}T}\sum_{ij}\left(3m_i A_{ji}\mu_{gj} + 3m_i A_{jj}\mu_{gi} - 2m_i A_{ij}\mu_{gj}\right)\left(3\cos^2\chi - 1\right) \\ & + \frac{1}{10k_\mathrm{B}T}\left(\alpha_{gm} - \overline{\alpha_g}\right)\left(3\cos^2\chi - 1\right) + \frac{\mu_g^{\,2}}{30k_\mathrm{B}^2T^2}\left(3\cos^2\alpha - 1\right)\left(3\cos^2\chi - 1\right) \end{aligned} \tag{1-9}$$

$$\begin{aligned} B_{3\cos^2\chi-1} = {} & \frac{1}{|\mathbf{m}|^2}\sum_{ij}\left(3m_i A_{ji}\Delta\mu_j + 3m_i A_{jj}\Delta\mu_i - 2m_i A_{ij}\Delta\mu_j\right)\left(3\cos^2\chi - 1\right) \\ & + \frac{3}{2}\left(\Delta\alpha_m - \overline{\Delta\alpha}\right)\left(3\cos^2\chi - 1\right) \\ & + \frac{1}{k_\mathrm{B}T}\left[3\left(\hat{\mathbf{m}}\cdot\boldsymbol{\mu}_g\right)\left(\hat{\mathbf{m}}\cdot\Delta\boldsymbol{\mu}\right) - \left(\boldsymbol{\mu}_g\cdot\Delta\boldsymbol{\mu}\right)\right]\left(3\cos^2\chi - 1\right) \end{aligned} \tag{1-10}$$

$$C_{3\cos^2\chi-1} = \left[3\left(\hat{\mathbf{m}}\cdot\Delta\boldsymbol{\mu}\right) - |\Delta\boldsymbol{\mu}|^2\right]\left(3\cos^2\chi - 1\right) \tag{1-11}$$

The χ-independent terms are

$$A_\mathrm{const} = \frac{1}{30|\mathbf{m}|^2}\sum_{ij}10A_{ij}^{\,2} + \frac{1}{15|\mathbf{m}|^2 k_\mathrm{B}T}\sum_{ij}10m_i A_{ij}\mu_{gj} \tag{1-12}$$

$$B_\mathrm{const} = \frac{1}{|\mathbf{m}|^2}\sum_{ij}m_i A_{ij}\Delta\mu_j + \frac{15}{2}\overline{\Delta\alpha} + \frac{5}{k_\mathrm{B}T}\left(\boldsymbol{\mu}_g\cdot\Delta\boldsymbol{\mu}\right) \tag{1-13}$$

$$C_\mathrm{const} = 5|\Delta\boldsymbol{\mu}|^2 \tag{1-14}$$

It follows from Eqs. 1-11 and 1-14 that $C_{3\cos^2\chi-1}$ and C_const cannot be independent. Assuming that $\Delta\boldsymbol{\mu}$ is parallel to $\boldsymbol{\mu}_g$, we get the relation $3\left(\hat{\mathbf{m}}\cdot\Delta\boldsymbol{\mu}\right) - |\Delta\boldsymbol{\mu}|^2 = |\Delta\boldsymbol{\mu}|^2\left(3\cos^2\alpha - 1\right)$, where α is the angle between the transition moment and the ground-state dipole moment. Thus, the constraint between $C_{3\cos^2\chi-1}$ and C_const is found to be

$$\frac{C_{3\cos^2\chi-1}}{C_\mathrm{const}} = \frac{1}{5}(3\cos^2\alpha - 1)(3\cos^2\chi - 1) = -\frac{2}{5}(1 - 3\cos^2\chi) \tag{1-15}$$

Here we used $\alpha = 0°$. In the actual fitting, the χ-independent component spectrum (Fig. 1-10b) was fit first, yielding the value of c_χ for the ν_s(OH) band, 4.22×10^{-3}. The fit was not good if we did not include the second derivative component. Using the relation Eq. 1-15, the value of c_χ for the ν_s(OH) band in the χ-dependent component spectrum was calculated to be -1.69×10^{-3}, which was then fixed during the fitting of the χ-dependent spectrum.

Using Eqs. 1-8 and 1-14, $|\Delta\boldsymbol{\mu}|$ is evaluated to be 8.1×10^{-4} D/f. Here f accounts for the difference between the strength of internal and external electric fields. It is usually smaller than unity in our experiments. For example, it was found to be about 0.6 in the previous work [12,13]. Taking the factor f into account, the value of $|\Delta\boldsymbol{\mu}|$ is of the order of 10^{-3} D. Andrews and Boxer [17] reported the values of $|\Delta\boldsymbol{\mu}|$ for the C≡N stretch modes of nitrile compounds embedded in frozen glass matrix, all of which are of the order of 10^{-2} D. The $|\Delta\boldsymbol{\mu}|$ value that we have obtained for the ν_s(OH) mode of water is one order of magnitude smaller than that for the C≡N stretch.

It will also be possible to evaluate $\overline{\Delta\alpha}$ and the tensor elements of **A** using Eqs. 1-12 and 1-13. However, the signal-to-noise ratio in our experiment is still not high enough to enable us to determine these quantities accurately. Improvement in data quality and more detailed quantitative analysis are left for the future studies.

1.4.2. Water in AOT reverse micelles [18]

Figure 1-12 shows the ΔA spectrum of water in the $w_0 = 15$ AOT reverse micelle ([AOT] = 0.30 M), together with the absorption spectrum measured with a 50-μm spacer. The external electric field strength was $F_{ext} = 2.9 \times 10^6$ V m^{-1}. To estimate the mean diameter and size distribution of the reverse micelles, dynamic light scattering was employed. The mean diameter d is obtained to be d =

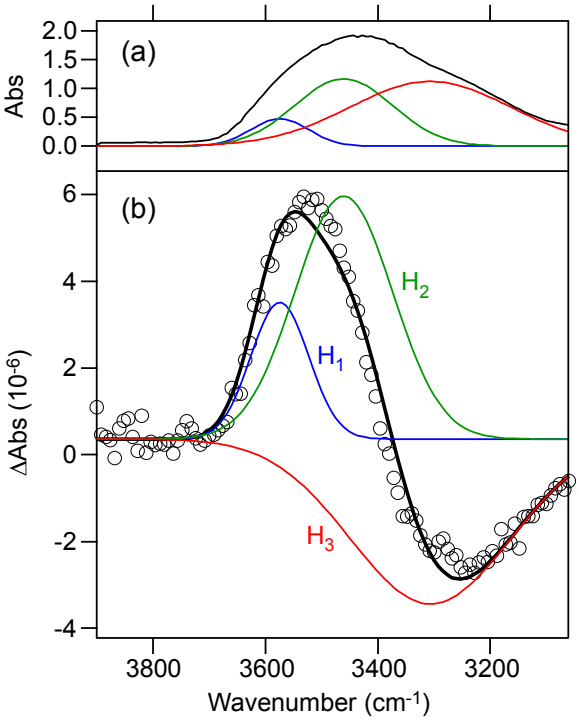

Figure 1-12: (a) ν(OH) spectrum of water in the $w_0 = 15$ AOT reverse micelle. The spectrum was fit to a superposition of three Gaussians (H_1, H_2, and H_3). (b) Observed ΔA spectrum (circles) and the best fit to Eq. 1-2 (black solid line).

6.4 (±1.0) nm, which is in reasonable agreement with the estimation d = 5.4 nm based on the empirical formula [10] $d = 0.29\ w_0 + 1.1$ (nm) with $w_0 = 15$.

As shown in Fig. 1-12a, the absorption spectrum was fit to a sum of three Gaussian subbands. This sharply contrasts with the case of water dissolved in 1,4-dioxane, for which Lorentzian functions give a better fit (see Fig. 1-7a). These subbands are thought of as representing water molecules in different hydrogen-bonding environments [19]. The subbands will be denoted H_1, H_2, and H_3 in order of decreasing the frequency. The peak position and band width (FWHM) of each component determined by the fitting are summarized in Table 1-4. With these parameters fixed, the ΔA spectrum was then fit to Eq. 1-2 including only the zeroth-derivative terms for the absorption bands H_1–H_3 (see Fig. 1-12b). Both absorption and ΔA spectra are well reproduced by assuming the three subbands. A simple calculation shows that the orientational anisotropy signal for a water molecule of μ_P = 1.85 D [20] is of the order of 10^{-7}, which is much smaller than the observed signal, so the ΔA signal can be attributed solely to a change in the equilibrium that is assumed to exist between H_1–H_3:

$$H_1 \underset{}{\overset{K_{12}}{\rightleftharpoons}} H_2 \overset{K_{23}}{\rightleftharpoons} H_3 \tag{1-16}$$

Table 1-4: Peak positions and band widths of Gaussian subbands H_1, H_2, and H_3 of water in the w_0 = 15 reverse micelles.

	Peak position (cm^{-1})		Band width (cm^{-1})
	This work	Previous work[a]	
H_1	3575 (±4)	3603 (±6)	73 (±5)
H_2	3461 (±6)	3465 (±5)	120 (±12)
H_3	3306 (±20)	3330 (±20)	200 (±12)

[a]Taken from reference [21]

The absorbance change ratios for components H_1–H_3 are determined as $(\Delta A/A)_{H1} = 6.4 \times 10^{-5}$, $(\Delta A/A)_{H2} = 4.6 \times 10^{-5}$, and $(\Delta A/A)_{H3} = -3.3 \times 10^{-6}$. Obviously the relation

$$\left(\frac{\Delta A}{A}\right)_{H_1} + \left(\frac{\Delta A}{A}\right)_{H_2} + \left(\frac{\Delta A}{A}\right)_{H_3} = 0 \tag{1-17}$$

does not hold, implying that the molar extinction coefficients of subbands H_1–H_3 are different due to different hydrogen-bonding configurations. The signs of $\Delta A/A$ for H_1–H_3 suggest that applying an electric field may cause hydrogen bonds to break (or weaken), giving rise to

apparent increase in the "bound water" (H_1 and H_2) and decrease in the "bulk water" (H_3) [6,8,21]. This result has an important implication that the chemical properties of confined water may be controlled by externally applying an electric field. The w_0 dependence of the ΔA spectrum will provide further support to our hypothesis and is left for future studies.

1.5. Summary and conclusions

In this work, we studied electric-field effects on the ν(OH) absorption of water in 1,4-dioxane and in AOT reverse micelles. In both cases, ν(OH) ΔA signals of water of the order of 10^{-6} has been successfully detected. To the best of our knowledge, our results are the first observation of IR electroabsorption of the ν(OH) transition of water. The IR spectrum in the 3000–3800 cm^{-1} range, of water in 1,4-dioxane is interpreted in terms of the symmetric and antisymmetric ν(OH) stretches of isolated water, which are well represented by Lorentzian bands. The angle χ dependence of the ΔA spectra strongly suggests significant contributions of the transition polarizability **A** to both χ-independent and χ-dependent ΔA spectra. In sharp contrast, the IR spectrum and ΔA spectrum of water in the w_0 = 15 AOT reverse micelle are well characterized by three Gaussian subbands (H_1, H_2, and H_3), indicating that the corresponding ν(OH) transitions are imhomogeneously broadened. Furthermore, the ΔA spectrum of water in the reverse micelle is dominated by the zeroth-derivative terms that originate not from **A** but from changes in equilibrium between H_1, H_2, and H_3. It is likely that the difference in the mechanism for the ν(OH) electroabsorption between the 1,4-dioxane solution and the reverse micelle stems from the local environment of water. In 1,4-dioxane solution (<2 M), most fraction of water molecules occurs as monomeric water that interacts mainly with 1,4-dioxane. The properties of such water molecules are thought to differ substantially from those in bulk, probably closer to those in the gas phase. Water in the reverse micelle is even more complicated. Although we have not collected enough data on this system, water in the w_0 = 15 reverse micelle seems to resemble neither isolated water nor bulk water. We believe the present study is an important first step to the research along this line.

2. Project II: Infrared electroabsorption spectroscopy of *N*,*N*-dimethyl-*p*-nitroaniline in acetonitrile and C_2Cl_4: Solvation of the solute and self-association of acetonitrile [14,22]

2.1. Introduction

Intermolecular interactions often give rise to molecular association. In solution, molecular association may take place between solute and solute, solute and solvent, or solvent and solvent, and profoundly affects the physicochemical properties of the solution, such as boiling point and dielectric constant. Thus it is of fundamental importance to elucidate molecular association in the solution phase and the underlying mechanisms. A sensitive probe of molecular association is the permanent dipole moment μ_P. Because the overall dipole moment of a given associated structure (*e.g.*, dimer) is the vector sum of those of the monomers that participate in the association, the dipole moment of the associated form should sharply reflects their relative orientation in space. For example, if two monomers align in a parallel manner, the resulting dipole would be approximately double that of the monomer. In contrast, the dipoles will be cancelled out if they align in an anti-parallel manner.

IR electroabsorption spectroscopy has proven very useful for probing permanent dipole moments in room-temperature solution [12–14]. When a polar molecule having the permanent dipole moment μ_P is subjected to an electric field, it undergoes reorientation along the field direction, giving rise to changes in IR absorbance. Our IR electroabsorption spectrometer, which combines a dispersive monochromator and an AC-coupled amplifier, enables detection of ΔA as small as 10^{-7}. The high potential of this apparatus has been demonstrated in the studies of *p*-nitroaniline (PNA) in acetonitrile (ACN) and CCl_4 [13] and liquid 1,2-dibromoethane [23].

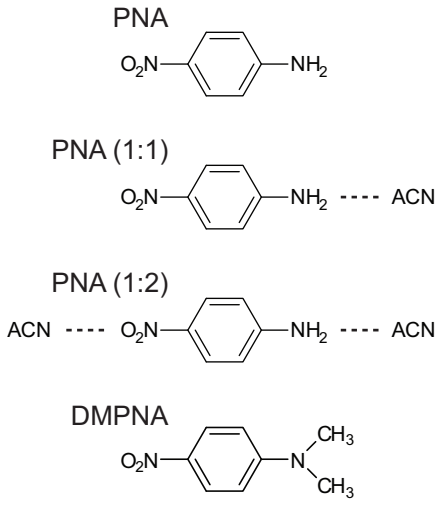

Figure 2-1: Chemical structures of PNA and DMPNA, and schematic of the 1:1 and 1:2 forms of PNA.

In the present study, we extended our previous work [13] on PNA to its derivative, *N*,*N*-dimethyl-*p*-nitroaniline (DMPNA), in ACN and C_2Cl_4. In our 2006 work [13], it is

shown that the two distinct solvated forms of PNA, *i.e.*, the 1:1 and 1:2 forms (see Fig. 2-1), have a head-to-tail linear structure. We ask the question of how substitution in PNA affects the formation of these solvated structures. In DMPNA, the hydrogen atoms in the NH_2 group are both replaced by the CH_3 group. To examine the effects of the *N*,*N*-dimethyl substitution, we focus on the NO_2 symmetric stretch $\nu_s(NO_2)$ in FT-IR and IR electroabsorption spectra.

2.2. Experimental

Experimental details have been given in Section 1.3.

2.3. Results and discussion

Figure 2-2 shows the ACN mole fraction (x_{ACN}) dependence of FT-IR spectra of PNA and DMPNA in ACN/C_2Cl_4 in the 1280–1360 cm^{-1} region. x_{ACN} was varied from 0.18 to 0.57, corresponding to 10 and 40 volume % of ACN, respectively. Two $\nu_s(NO_2)$ bands are observed in the PNA spectra (Fig. 2-2a); the higher-wavenumber band is attributed to the 1:1 form, and the lower-wavenumber band to the 1:2 form [24]. As x_{ACN} increases, the 1:1 band decreases with a slight peak shift, whereas the 1:2 form increases without any appreciable shift. This observation has been interpreted as being a consequence of population changes in equilibrium between the 1:1 and 1:2 forms. As opposed to PNA, the $\nu_s(NO_2)$ band of DMPNA (Fig. 2-2b) appears to be a single broad band and to undergo a continuous redshift with increasing x_{ACN}. This behavior, which is typical of the so-called solvent effect, leads us to a hypothesis that DMPNA does not form specific solvated structures with ACN.

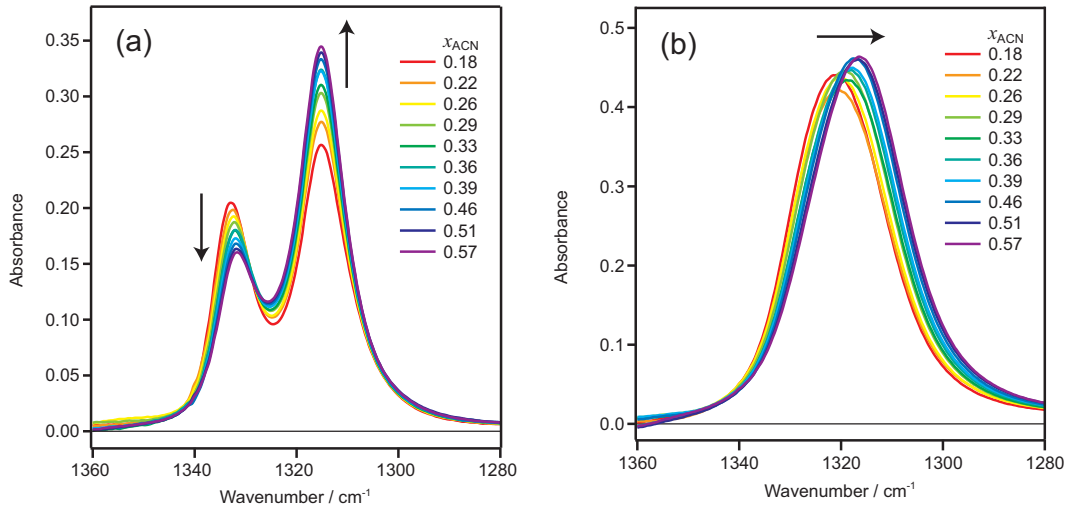

Figure 2-2: FTIR spectra of PNA (a) and DMPNA (b) in ACN/C_2Cl_4 at 10 different mole fractions of ACN, x_{ACN}. The concentration of PNA and DMPNA was 30 mM.

To provide further evidence for the absence of the solvation of DMPNA, we measured the χ dependence of IR electroabsorption spectra of DMPNA in ACN/C_2Cl_4 (x_{ACN} = 0.18), where χ is the angle between the applied electric field and the polarization of the incident IR light (Fig. 2-3). In the IR spectrum (Fig. 2-3a), three vibrational transitions are seen; in order of decreasing wavenumber, the CH_3 symmetric deformation, $\delta_s(CH_3)$, of ACN, an combination band of C_2Cl_4 [25], and $\nu_s(NO_2)$ of DMPNA. In Fig. 2-3b, the $\nu_s(NO_2)$ band shows a large negative signal, which decreases gradually in intensity on going from χ = 90° to 55°. The χ = 55° spectrum of DMPNA is quite different from that of PNA (data not shown), which shows a dispersive feature arising from field-induced equilibrium shift from the 1:1 form to the 1:2 form. The SVD of the χ-dependent spectra of DMPNA yields one principal singular value, and the spectra can be reproduced fairly well by assuming this component only (dashed curves in Fig. 2-3b). Taken together, the FT-IR and χ-dependent electroabsorption results indicate that, as opposed to PNA, DMPNA forms no specific solvated structures in ACN/C_2Cl_4 and behaves as the monomer. Whether the solute forms solvated species in solution or not may significantly affect the reactivity of the solute in chemical reactions. Our present study has demonstrated the power of IR electroabsorption spectroscopy in this regard.

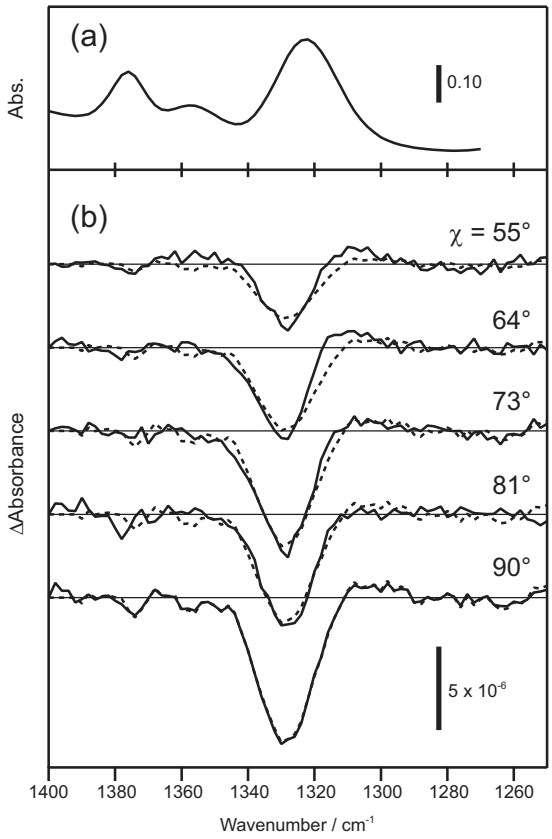

Figure 2-3: Absorption spectrum (a) and χ-dependent ΔA spectra (b) of DMPNA in ACN/C_2Cl_4 (x_{ACN} = 0.18). The dashed curves represent the reproduced spectra by assuming only a single component.

Careful inspection of the ΔA spectra in Fig. 2-3b reveals a weak ΔA signal of $\delta_s(CH_3)$ at around 1375 cm^{-1}. To obtain ΔA spectra with higher signal-to-noise ratio, we averaged more scans at the cost of the number of measurement angle χ. The ΔA spectra so obtained are

displayed in Fig. 2-4. The ΔA signal of $\delta_s(CH_3)$ is now evident in Fig. 2-4b. To analyze the ΔA spectra, we first fit the absorption spectrum (Fig. 2-4a) to the sum of three Gaussian functions, which account for $\delta_s(CH_3)$ of ACN, the combination band of C_2Cl_4, and $\nu_s(NO_2)$ of DMPNA. Subsequently, we fit the ΔA spectra at χ = 90° and 55° to Eq. 1-2, in which we considered only the $\delta_s(CH_3)$ and $\nu_s(NO_2)$ modes with their peak position and band width fixed. This is because the contribution of the C_2Cl_4 band to the ΔA spectra is negligibly small. As can be seen in Fig. 2-4b, Eq. 1-2 does a good job of fitting the observed ΔA spectra. The zeroth derivative signal of the χ-dependent component arises from orientational polarization and is related to the permanent dipole moment of the molecular species as

$$\frac{\Delta A}{A} = \frac{1}{30}\left(\frac{\mu_P F}{k_B T}\right)^2 (1-3\cos^2\chi)(1-3\cos^2\eta) \qquad (2\text{-}1)$$

where F is the *internal* field strength, k_B is the Boltzmann constant, T is temperature, and η is the angle between μ_P and the transition moment. Using Eq. 2-1 with known values of F, T, χ, and η, the value of μ_P can be calculated from the observed ΔA signal. In practice, however, it is very difficult to do so because the field strength F cannot be estimated accurately in most cases. A potent resolution for this problem is to use an intensity standard. In the present case, the ΔA signal of DMPNA can serve as an internal intensity standard to calculate the dipole moment of ACN. It follows from Eq. 2-1 that

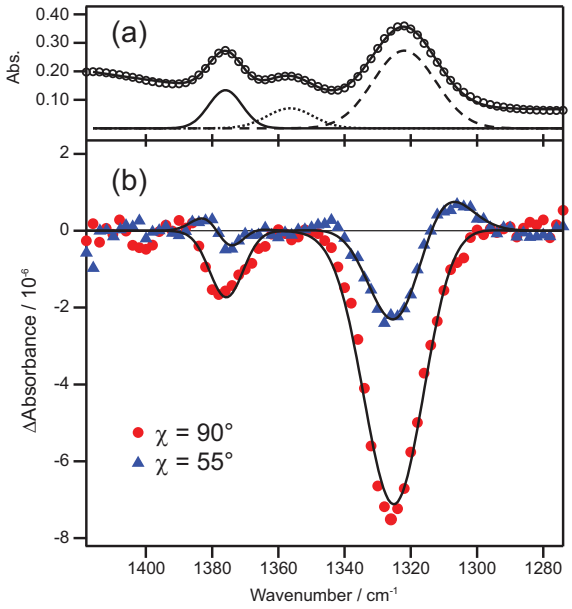

Figure 2-4: Fitted results of the absorption spectrum (a) and ΔA spectra (b) of DMPNA in ACN/C_2Cl_4 (x_{ACN} = 0.18). In (a), the absorption spectrum is fit to the sum of three Gaussian bands plus a baseline.

$$(\Delta A / A)_{ACN} / (\Delta A / A)_{DMPNA} = \left(\mu_P^{ACN} / \mu_P^{DMPNA}\right)^2 \qquad (2\text{-}2)$$

Note that the field strength F no longer appears in Eq. 2-2, hence the dipole moment can be evaluated free from uncertainty in F. Because DMPNA has been shown to form no solvated structures with ACN, the dipole moment of the DMPNA monomer can be used as μ_P^{DMPNA}.

Here we use a literature value of μ_P^{DMPNA} in dilute benzene solution, μ_P^{DMPNA} = 7.0 D. From the fitting of the ΔA spectra in Fig. 2-4b, we obtain $(\Delta A/A)_{ACN} = -1.3 \times 10^{-5}$ and $(\Delta A/A)_{DMPNA} = -2.0 \times 10^{-5}$. Substituting these values into Eq. 2-2, we obtain μ_P^{ACN} = 5.7 D.

The experimentally determined μ_P^{ACN} is about 1.7 times larger than that of the ACN monomer (3.43 D in dilute CCl_4 solution [3]). This discrepancy cannot be accounted for by experimental errors, but rather it is attributed to self-association of ACN. Considering the low mole fraction of ACN in the binary mixture studied, a dimer is most likely to occur in the solution. Two types of dimer structures of ACN have been discussed; an anti-parallel dimer [26] and a head-to-tail linear dimer [27,28]. In an anti-parallel dimer (Fig. 2-5a), two ACN molecules interact with one another via the C–C≡N part and align side by side in the opposite direction such that their dipole moments cancel out. Thus the resulting dipole moment of the dimer would be zero. In contrast, in a linear dimer (Fig. 2-5b), two ACN molecules align in a head-to-tail manner resulting in the overall dipole moment of ~6.8 D. Although *ab initio* molecular orbital calculations [28] reveal that the linear dimer structure is higher in energy than the anti-parallel structure, our result is in favor of the linear dimer.

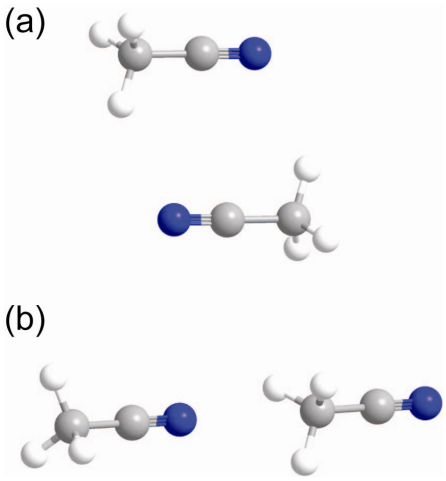

Figure 2-5: Anti-parallel (a) and head-to-tail linear (b) dimer structures.

2.4. Conclusions

We used IR electroabsorption and FTIR spectroscopies to study solvated structures of DMPNA in binary mixtures of ACN and C_2Cl_4. In comparison with PNA, DMPNA was found to occur as a monomer rather than as specific solvated structures with ACN. This finding illustrates that *N*,*N*-dimethyl substitution in the NH_2 group profoundly affects the intermolecular interaction in the solution. Similar effects are anticipated for other types of substitution such as replacing hydrogen atom(s) in the aromatic ring. We also analyzed the ΔA signal of ACN in detail and found that a head-to-tail linear dimer (Fig. 2-5b) is most likely to occur in the solution studied. Apparently this picture contradicts the *ab initio* calculation result [28] where the anti-parallel structure has been shown to be more stable than the linear structure. However it was obtained in gas-phase calculations. In an environment in which

ACN is surrounded by C_2Cl_4, the local polarity induced by polarizable C–Cl bonds of C_2Cl_4 could possibly stabilize polar linear dimers to a greater extent than nonpolar anti-parallel dimers. Finally it is important to note that the associated structures in solution which we have discussed should not be viewed as being rigid and well-defined, as opposed to those in the gas phase. In other words, they are continuously being subject to intermolecular interactions with the surrounding and fluctuating over time. Thus, the linear-dimer structure of ACN revealed in this work may be more appropriately expressed as an averaged picture of fluctuating structures of ACN aggregates.

參考文獻

[1] W. Liptay, Dipole Moments and Polarizabilities of Molecules in Excited Electronic States. In *Excited States*; E. C. Lim, Ed.; Academic Press: New York and London, 1974; pp 129; W. Liptay, *Angew. Chem. Int. Ed.* **8**, 177 (1969).

[2] G. U. Bublitz and S. G. Boxer, *Annu. Rev. Phys. Chem.* **48**, 213 (1997).

[3] A. L. McClellan, *Tables of Experimental Dipole Moments*; W. H. Freeman and Company: San Francisco, 1963.

[4] M. L. Cowan, B. D. Bruner, N. Huse, J. R. Dwyer, B. Chugh, E. T. J. Nibbering, T. Elsaesser, and R. J. D. Miller, *Nature*, **434**, 199 (2005).

[5] N. Levinger, *Science*, **298**, 1722 (2002).

[6] G. Onori and A. Santucci, *J. Phys. Chem.* **97**, 5430 (1993).

[7] J. C. Dèak, Y. Pang, T. D. Sechler, Z. Wang, and D. D. Dlott, *Science*, **306**, 473 (2004).

[8] S. Balakrishnan, N. Javid, H. Weingärtner, and R. Winter, *ChemPhysChem*, **9**, 2794 (2008).

[9] S. Ray and S. P. Moulik, *Langmuir*, **10**, 2511 (1994).

[10] Kinugasa, A. Kondo, S. Nishimura, Y. Miyauchi, Y. Nishii, K. Watanabe, and H. Takeuchi, *Colloids Surf. A* **204**, 193 (2002).

[11] S. A. Locknar and L. A. Peteanu, *J. Phys. Chem. B* **102**, 4240 (1998).

[12] H. Hiramatsu and H. Hamaguchi, *Appl. Spectrosc.* **58**, 355 (2004).

[13] S. Shigeto, H. Hiramatsu, and H. Hamaguchi, *J. Phys. Chem. A* **110**, 3738 (2006).

[14] W.-C. Wang and S. Shigeto, *J. Phys. Chem. A* **115**, 4448 (2011).

[15] 史習岡，研究水溶解於 1,4-二氧陸圜的電場變調紅外線吸收光譜學，國立交通大學分子科學研究所碩士論文(2011).

[16] D. D. Lee and H. S. Seung, *Nature*, **401**, 788 (1999).

[17] S. S. Andrews and S. G. Boxer, *J. Phys. Chem. A* **104**, 11853 (2000).

[18] 李依純，利用電場變調紅外線吸收光譜研究化學平衡：從簡單的液體系統到複雜的油包水乳液，國立交通大學分子科學研究所碩士論文(2009).

[19] A. Rahman and F. H. Stillinger, *J. Chem. Phys.* **55**, 3336 (1971); R. Laenen, R. Rauscher, and A. Laubereau, *J. Phys. Chem. B* **102**, 9304 (1998).

[20] S. A. Clough, Y. Beers, G. P. Klein, and L. S. Rothman, *J. Chem. Phys.* **59**, 2254

(1973).

[21] N. V. Nucci and J. M. Vanderkooi, *J. Phys. Chem. B* **109**, 18301 (2005).

[22] 王威傑，利用電場調變紅外線吸收光譜研究 *N,N*-Dimethyl-*p*-nitroaniline 在混合溶液乙晴和四氯乙烯中溶質的溶解和乙晴的結構，國立交通大學應用化學所碩士論文(2010).

[23] I-C. Lee, H. Hamaguchi, and S. Shigeto, *Chem. Phys. Lett.* **466**, 144 (2008).

[24] K. Mohanalingam, D. Yokoyama, C. Kato, and H. Hamaguchi, *Bull. Chem. Soc. Jpn.* **72**, 389 (1999).

[25] H. J. Bernstein, *J. Chem. Phys.* **18**, 478 (1950).

[26] B. H. Thomas and W. J. Orville-Thomas, *J. Mol. Struct.* **3**, 191 (1969); E. Knözinger and D. Leutloff, *J. Chem. Phys.* **74**, 4812 (1981); T. Takamuku, M. Tabata, A. Yamaguchi, J. Nishimoto, M. Kumamoto, H. Wakita, and T. Yamaguchi, *J. Phys. Chem. B* **102**, 8880 (1998); T. B. Freedman and E. R. Nixon, *Spectrochim. Acta A* **28**, 1375 (1972).

[27] W. R. Fawcett, G. Liu, and T. E. Kessler, *J. Phys. Chem.* **97**, 9293 (1993); C. E. H. Dessent, J. Kim, and M. A. Johnson, *J. Phys. Chem.* **100**, 12 (1996).

[28] E. M. Cabaleiro-Lago and M. A. Rìos, *J. Phys. Chem. A* **101**, 8327 (1997).

附錄

List of papers based on work supported by the present research grant:

1. Sohshi Yabumoto, Shinsuke Shigeto*, Yuan-Pern Lee, and Hiro-o Hamaguchi*, November 2010, "Ordering, Interaction, and Reactivity of the Low-Lying nπ* and ππ* Excited Triplet States of Acetophenone Derivatives", *Angew. Chem. Int. Ed.* **49**, 9201–9205 (2010). IF = 12.73
2. Wei-Chieh Wang and Shinsuke Shigeto*, May 2011, "Infrared Electroabsorption Spectroscopy of *N*,*N*-Dimethyl-*p*-nitroaniline in Acetonitrile/C_2Cl_4: Solvation of the Solute and Self-Association of Acetonitrile", *J. Phys. Chem. A* **115**, 4448–4456 (2011). IF = 2.732